11

Co/Cu Nanowire Systems for GMR Sensing Applications

Daniele Pullini[1], David Busquets Mataix[2] and Alessio Tommasi[1,2]
[1]*Centro Ricerche Fiat,*
[2]*Universidad Politécnica de Valencia,*
[1]*Italy*
[2]*Spain*

1. Introduction

Since the discovery of giant magnetoresistance (GMR) in 1988 by Albert Fert and Peter Grünberg many companies have sought to develop practical applications for this intriguing effect of magnetic multilayer stacks. The applications of magnetic multilayer stacks are diverse, but in general they can serve as: magnetic field sensors (Simonds, 1995; Grünberg et al., 1986; Saurenbach et al., 1988; Baibich et al., 1988), non-volatile memories (Manalis et al., 1995; Chou et al., 1994), or variable resistors when small magnetic fields have to be measured. The first GMR sensor commercially available was introduced in 1995 by NVE Corporation. Since then, users can rely on a large variety of devices exploiting GMR: analogue and digital sensors, switches, gradient transducers for contactless positioning systems, e.g. gear tooth and encoder applications. Today, it is generally acknowledged that GMR sensors outperform the competing technologies such as AMR and Hall virtually in every application, and often at a significantly lower cost. The conventional GMR stacks are produced by vacuum deposition technology; more specifically, by this technique, a large variety of thin film materials are serially deposited, within a single vacuum chamber, one on top of another, to form multilayer stacks of tailored magnetic properties. The need to accurately control the nanometric thickness of each film, their extremely low roughness, and their purity do majorly contribute to the final cost of this type of systems. For this reason, the use of these devices, especially in low-margin markets such as the automotive, is still prohibitive for a number of potential field applications. In this context, alternative processes are envisaged to lower the final cost of GMR sensors. To this end, the pulsed electrodeposition into nanoporous templates (hereinafter template pulsed electrodepostion, TPED) is presented here as a competitive alternative to mass produce GMR sensors in the form of arrays of multilayer nanowires. As being a promising candidate for a low-cost production of sensors tailored for the aforementioned field uses (Pullini et al., 2007a), Co/Cu multilayer nanowire arrays fabricated by TPED (Fert & Piraux, 1999; Piraux et al., 1994) are discussed in this chapter. Specifically, the present chapter aims at presenting the criteria to model, design, develop Co/Cu-multilayer nanowire arrays, and discuss their potential exploitation perspectives to be used as magnetic field sensors.

In a first part of this chapter a quasi-analytical analysis (QAD) of cylindrical Co/Cu/Co tri-layer systems is detailed, and the equations drew to calculate the critical fields, the linearity,

and the eccentricity of their re-magnetization characteristics are reported. Systems differing by diameter, easy-axis, thickness of each layer employed are classified accordingly in order to provide to an end-user with the most significant choice parameters to fulfill a custom application. Micromagnetic simulation is then used to corroborate the QAD predicted properties for a large plurality of elementary trilayers and to simulate the magnetic behaviour of selected interacting trilayers both when piled up to form nanowires (up to 50 Co/Cu bilayers) and arranged in parallel, on the same plane, to mimic nanowire arrays (5 x 3 array).
The second part of the chapter is focused on TPED; in particular, this technique is here described and the most important parameters allowing the tailoring of the system characteristics are highlighted and their variability ranges detailed and linked to morphological, structural and magnetic properties. In particular, from a suitable electrolyte composition, the electrode potential, the current density, and the deposition temporization to be used in an pulsing regime to grow Co and Cu thin layers within nanoporous templates are reported. Always in this section, a description of the best practice to get large quantities of filled nanopores per area as well as large current efficiency is given.

2. Quasi-analytical modeling of Co/Cu/Co trilayer systems

The aim of the present section is to propose a rational for designing and classifying, as a function of selected parameters, cylindrical Co/Cu/Co trilayer systems of different diameters to have an insight into the properties of more complex nanowire based systems to be used for building magnetic field sensors (Ohgai et al., 2003). It is important to clarify here that the Co/Cu/Co trilayer has been considered instead of the Co/Cu nanowire's elementary-cell, that is the bilayer, in order to take into account the contribution of the interlayer exchange coupling energy to the system's total energy, which does not exist in an elementary bilayer.
To design such a system one can rely on different methods: phenomenological modeling from the experimental characterization and testing of physical samples, analytical modeling, and micromagnetic simulation, by which the rotation of the single dipoles can be described. Among these approaches, experimental is time consuming, theory is usually limited to verifying the correctness of the assumptions, while simulation is a helpful tool to be used when theory gives ambiguous responses (e.g. saddle points on the system's energy surface) and the experimental measures are not fully repeatable due to the size and shape dispersion of the nano-object samples fabricated very often in few units. According to the device addressed, whether being a sensor, a memory cell, or a magnetometer, the response to an applied magnetic field of an elementary Co/Cu/Co trilayer system has to be predicted with satisfactory confidence to justify the massive experimental workload typically needed for their development.
In principle, the responses of these systems have to be very different from one another according to the diverse applications; in fact, if a memory element is targeted a bistable hysteresis loop is desirable, while if a magnetic field sensor is wanted, one prefers to deal with a symmetric GMR and a linear analogue response within a defined dynamic range of operation. Generally speaking, elementary Co/Cu/Co trilayer systems show a symmetric GMR when they are in the parallel states of magnetization at the saturation field and their remanence is zero in the absence of a magnetic field applied. Differing in geometry parameters and material characteristics, the number of diverse systems exhibiting such a behaviour is huge; therefore, since the present chapter specifically refers to sensing

applications, to circumscribe the investigation, those systems whose first magnetization curve starts from zero in the absence of an applied field were searched for – these systems satisfy what is referred here as zero-field condition (hereinafter ZFC). The ZFC as well as the hysteresis characteristics of these systems depends on many factors such as the diameter (d), the thicknesses (t_{Cu}, t_{Co}), and crystal orientations of the separate layers. In the present work, in order to find the most useful systems, the energy problem of cylindrical Co/Cu/Co trilayers as a function of the magnetocrystalline-anisotropy easy-axis direction (hereinafter a), d, t_{Cu}, and t_{Co}, and their dynamic response to a changing applied field is studied. Specifically, to solve the energy problem in the ZFC, and to estimate the coercivity and saturation fields of cylindrical Co/Cu/Co trilayers a quasi-analytical design (QAD) approach was defined and adopted instead of running time consuming micromagnetic simulation. In the frame of the QAD, the demagnetization energy values of the elementary trilayer when in the fundamental configurations of magnetization (when the single layers' magnetizations are parallel/antiparallel to one another and to the trilayer plane respectively) were calculated numerically and used to interpolate the analytical expression of the demagnetization energy as a part of the analytical expression of the system's total energy. When the systems satisfying the ZFC were found, and their critical fields calculated in this way, the micromagnetic simulation was carried out for these selected systems to verify the QAD predictions and to know the systems' dynamic behaviour. As a result, a systemic data framework was completed to aid the design of custom Co/Cu/Co trilayer systems for the diverse sensing applications.

The prediction of the critical fields in the magnetization process results from the analysis of the total energy of the system. The energies involved in the Co/Cu/Co trilayer system are exchange, Zeeman, demagnetization, magnetocrystalline anisotropy, and RKKY interlayer exchange coupling energy. In order to find the systems which satisfy the ZFC, as well as to predict their critical fields, the system's total energy is defined by assuming that the-least-energy states occur when the magnetic moments belonging to each magnetic layer are lined up. This assumption leads to:

$$E_{ex} = 0. \tag{1}$$

The Zeeman energy is given by:

$$E_z = M_s H V_{Co} \left[(\mathbf{m_1} \cdot \mathbf{h}) + (\mathbf{m_2} \cdot \mathbf{h}) \right], \tag{2}$$

where $M_s\mathbf{m_1}$ and $M_s\mathbf{m_2}$ are the magnetizatio n of the top and bottom layer respectively and H**h** is the applied magnetic field considered uniform over the system volume. The magnetocrystalline anisotropy of cobalt is uniaxial in most the fabricated systems reported in the literature (Sun et al., 2005) and it can be written as follows:

$$E_{anis} = K_1 V_{Co} \left(|\mathbf{m_1} \times \mathbf{a}|^2 + |\mathbf{m_2} \times \mathbf{a}|^2 \right), \tag{3}$$

where K_1 is the anisotropy constant and V_{Co} is the volume of the cobalt layer. Two magnetic layers spaced by a thin non-magnetic layer experience RKKY interlayer exchange coupling, which is described by the following energy term:

$$E_{IEC} = I_{12}(t_{Cu}) 2 A_{Co} (\mathbf{m_1} \cdot \mathbf{m_2}), \tag{4}$$

where A_{Co} is the area of the Co/Cu interface and I_{12} is the interlayer coupling constant (Bruno & Chappert, 1991) and is dependent on the thickness and orientation of the spacer layer (copper in the present work). The demagnetization energy is given by:

$$E_d = -\iiint_{V_{Co}} \mathbf{M} \cdot \iint_{A_{Co}} \mathbf{M} \cdot \mathbf{n} \frac{\mathbf{r}-\mathbf{r}'}{\left|\mathbf{r}-\mathbf{r}'\right|^3} d^2\mathbf{r}' d^3\mathbf{r}. \quad (5)$$

This expression can be approximated empirically by fitting with a linear function the values, calculated numerically, of the demagnetization energy of the system when in four fundamental states of magnetization. As a result, the following expression was found:

$$E_{demag} = \frac{1}{2}\left[\Delta E_{d_{||}} \mathbf{m_{1}}_{||} \cdot \mathbf{m_{2}}_{||} + \Delta E_{d_{\perp}} \mathbf{m_{1}}_{\perp} \cdot \mathbf{m_{2}}_{\perp} + \left(\Sigma E_{d_{\perp}} - \Sigma E_{d_{||}} \right) \left(\left|\mathbf{m_{1}}_{\perp}\right|^2 + \left|\mathbf{m_{2}}_{\perp}\right|^2 \right) \right], \quad (6)$$

where $\mathbf{m_i}_{||}$ and $\mathbf{m_i}_{\perp}$ denote respectively the in-plane and perpendicular-to-plane components of $\mathbf{m_i}$ and $\Delta E_{d||} \equiv E_{d,P||} - E_{d,AP||}$, $\Delta E_{d\perp} \equiv E_{d,P\perp} - E_{d,AP\perp}$, $\sum E_{d\perp} \equiv E_{d,P\perp} + E_{d,AP\perp}$, and $\sum E_{d||} \equiv E_{d,P||} + E_{d,AP||}$ are coefficients linked to the demagnetization energy of a trilayer system when the Co layers are in the parallel/antiparallel configurations of magnetization, here indexed P/AP, and when their magnetizations are both parallel/orthogonal to the trilayer plane, here indexed ||/⊥. The coefficients aforementioned depend on the dimensions of the layers as they were interpolated from the calculated values of e_d, the energy per magnetic volume, as a function of t_{Co} / d and t_{Cu} / d. It was supposed that the system's layers are parallel to the xy-plane and the applied field is lined up along the x direction. The magnetocrystalline easy-axis, which is directly related to the crystal phase of the magnetic layers, can lie, in principle, along any direction depending on the lattice orientation of the deposited cobalt, and the system's hysteresis loop reflects a clear uniaxial-anisotropy behaviour. A simple test of correlation between the quasi-analytical predictions and the micromagnetic simulations was carried out at zero field applied; in particular, the evolution towards the equilibrium state of the systems which satisfies, and do not satisfy, the ZFC were simulated and verified. In this context, the system was assumed to be unmagnetized as initial condition and let evolve to the least energy state. To predict the equilibrium state of these systems at zero field we evaluated in which state of magnetization the system's total energy is the smallest. The simplest case is when the magnetocrystalline easy-axis is lined up along the same direction of the demagnetization one (here the x direction), therefore, only the P and AP in-plane magnetizations are candidates. In particular, the system is in the P state if:

$$4 A_{Co} I_{12} > \Delta E_{d_{||}}, \quad (7)$$

meaning when the interlayer exchange coupling is sufficiently ferromagnetic to overcome the demagnetization, the latter tending to cause AP configuration. From equation (7), the parameters defining the geometry of the trilayer systems which satisfy the ZFC can be calculated. In a next step of our investigation the magnetization states of the systems which satisfy the ZFC were calculated in the presence of increasing applied magnetic field in the x direction. Then the equation $dE/d\mathbf{m_1} = 0$ was solved in order to localize the systems' energy minima; as a result, it was found that the top layer flips either exclusively in the xy-plane (||) or exclusively in the xz-plane (⊥) when the applied field is sufficiently intense. The flip

fields: $H_{||}$, $H\perp$ (relative to both the flip directions) can be calculated by solving: $d^2E / d\mathbf{m_1}^2 = 0$; it should not astonish that the flip process which occurs correspond to an applied field equal to $H_c = \min(H_{||}, H\perp)$, where $H_{||}$ and $H\perp$ are solutions of: $d^2E / d\mathbf{m_{1||}}^2 = 0$ and $d^2E / d\mathbf{m_1}\perp^2 = 0$, and they are respectively:

$$H_{||} = \frac{\Delta E_{d_{||}} + 4\,A_{Co} I_{12} + 4K_1 V_{Co}}{2M_s V_{Co}}, \tag{8}$$

$$H_{\perp} = \frac{\left(E_{d,AP_{\perp}} - E_{d,AP_{||}}\right) + \left(E_{d,P_{\perp}} - E_{d,P_{||}}\right) + 4\,A_{Co} I_{12} + 4K_1 V_{Co}}{2M_s V_{Co}}. \tag{9}$$

Analogously, when the easy-axis is oriented along the z direction we have the following expressions:

$$H_{||} = \frac{\Delta E_{d_{||}} + 4\,A_{Co} I_{12}}{2M_s V_{Co}}, \tag{10}$$

$$H_{\perp} = \frac{\left(E_{d,P_{||}} - E_{d,AP_{\perp}}\right) + \left(E_{d,P_{||}} - E_{d,P_{\perp}}\right) + 4A_{Co} I_{12} + 4K_1 V_{Co}}{2M_s V_{Co}}. \tag{11}$$

3. Behaviour simulation

To simulate the dynamics of magnetization of Co/Cu/Co trilayer systems the Object Oriented Micro-Magnetic Framework (OOMMF) software package developed by NIST was used. In this framework, the cobalt layers can be represented by magnetic discs while the copper layer, being non-magnetic, is considered a part of the surroundings. The lattice orientation of copper is reflected in the function $I_{12}(t_{Cu})$ (Bruno & Chappert, 1991); however, this paper discusses only the (111) orientation of copper as this crystal order is more frequently reported in the literature experiments (Tan & Stadler, 2006; Jyoko et al., 1997). Concerning cobalt, the structure more frequently reported in the literature is the *hcp* although this material can also be grown as *fcc* by electrodeposition and other techniques. For this reason, the exchange stiffness and magnetocrystalline anisotropy of cobalt *hcp* have been used here and the respective values are given in Table 1.

The *c-axis* of *hcp* cobalt is the easy-axis of magnetization; therefore, when detailing the Co easy-axis orientation in the simulator framework, this point has to be carefully taken into account to avoid simulating systems which eventually cannot be fabricated for practical reasons. However, seeing that Piraux and co. demonstrated that the *c-axis* direction of *hcp* cobalt can be controlled by process parameters when the material is grown into nanoporous templates by electrodeposition we considered here the easy-axis of Co oriented along the *x* and *z* directions (Piraux et al., 1994).

Magnetocrystalline anisotropy, K_1	4.5×10^5 J/m^3 [a]
Exchange stiffness, A	28×10^{-12} J/m [b]
Saturation magnetization, M_s	1.4459×10^6 A/m [a]

Table 1. Values of parameters given to the cobalt layers.

In this section only the systems which satisfy the ZFC are concerned, and for these systems, the dynamic behaviour is simulated by sweeping the applied field, from zero, towards the +/-*x* direction; therefore, if initially, in the absence of applied field, the system's bottom layer is magnetized along the +*x* direction its top layer must be magnetized along the –*x* one. From this condition, an external magnetic field is applied along the +*x* axis and, as a consequence, only the top layer can flip from its original orientation towards the +x direction over the course of the simulation. In particular, the applied field is increased of intensity in small steps (minimum step: 1 Oe), and for each field the system evolves to the equilibrium. The OOMMF can calculate, at each incremental step, the system evolution in two different ways: (i) by solving the Landau-Lifshitz (LL) equations (time driver method, hereinafter TD) or (ii) by searching for the nearest energy minimum by using a conjugate gradient minimizer (minimization driver method, hereinafter MD). The use of the TD is proper when knowing the remagnetization dynamics towards the equilibrium is needed and, as a result, the single magnetic moment precession in the time domain can be visualized (for these cases a damping constant equal to 0.5 was used). Unfortunately, this method is time consuming, and it is not worthwhile to use it when one is only interested in localizing the equilibrium final state; in this case instead, the MD is more convenient as it is considerably faster. A concern about MD, however, is that due to the nature of the algorithm implemented, the system tends to stay in the energy saddle point of the AP state, or similarly in the –P state at the top of the energy hill, while the TD algorithm lets the system precess out of the saddle. In other words, in the former case, the system tends to persist in a previous equilibrium state even when the applied field is significantly changed, a fact which results in a misleading prediction of the system's hysteresis loop (the prediction error of the flip field can also be as large as 10% for particular systems). In the present work, this problem was solved by adding a random noise field to the system in the MD case to break the symmetry explicitly.

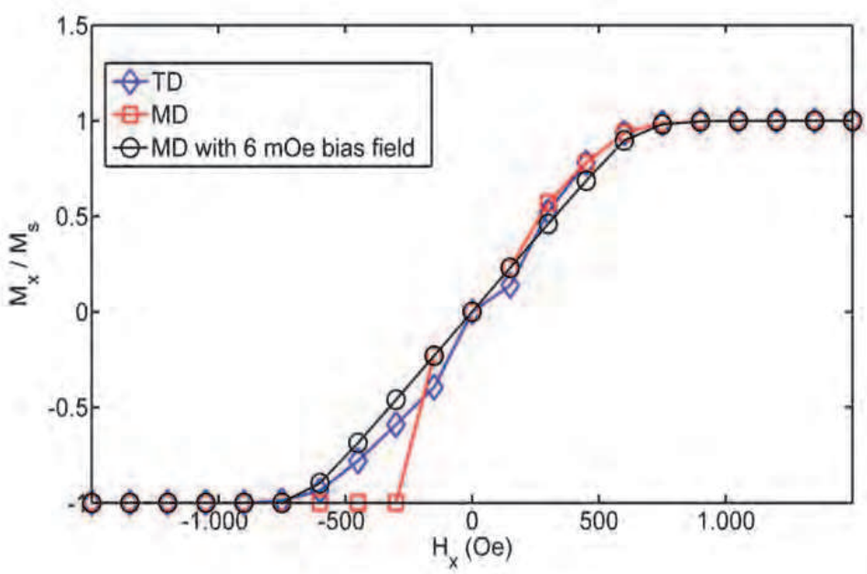

Fig. 1. Normalized magnetization curves of a Co/Cu/Co trilayer system of: d = 700 nm, t_{Co} = 1 nm, t_{Cu} = 2 nm and easy-axis oriented along the z direction.

The MD approach was used here with a quantified random noise which allowed us to estimate, saving more than 90% of computational time, the critical fields calculated by the TD. For a specific system, Figure 1 shows the effect of a 6 mOe field (random noise) on the predictions of the magnetization curve previously calculated by the TD. In terms of orders of magnitude, the intensity of the random noise used in this case is 10^{-6} smaller than the field to be applied to change the system magnetization (H_{sat}, about -800 Oe in the figure example), value corresponding to the maximum error committed when the flip field is calculated through the biased MD instead of the TD. In particular, in the Figure 1 the phenomenon of magnetization persistence when MD is used without random noise (square-dot curve) is represented.

3.1 Correlation domain between quasi-analytical prediction and micromagnetic simulation

To have a clue of the degree of confidence in using the quasi-analytical approach to predict the critical fields of a trilayer system, the coercivity and saturation fields of a large variety of system configurations of diameter 100 nm and differing in t_{Co} (from 1 to 40 nm) and t_{Cu} (from 3 to 40 Å) were calculated by QAD and compared with the relative output values of the OOMFF simulation. From the simulations performed it was noted that when the easy-axis of the magnetocrystalline anisotropy is oriented along the same direction of the applied field the flip from AP to P is immediate, therefore, the correlation analysis is reported here for easy-axis oriented along the *x* direction to show the accordance grade between modeling and simulation and to gauge their discrepancies; in fact, for this specific case, H_c and H_{sat} are coincident and give an unequivocal measurement of the switching field. In Figure 2 the switching fields calculated by QAD and the corresponding values calculated by OOMMF are reported for these systems.

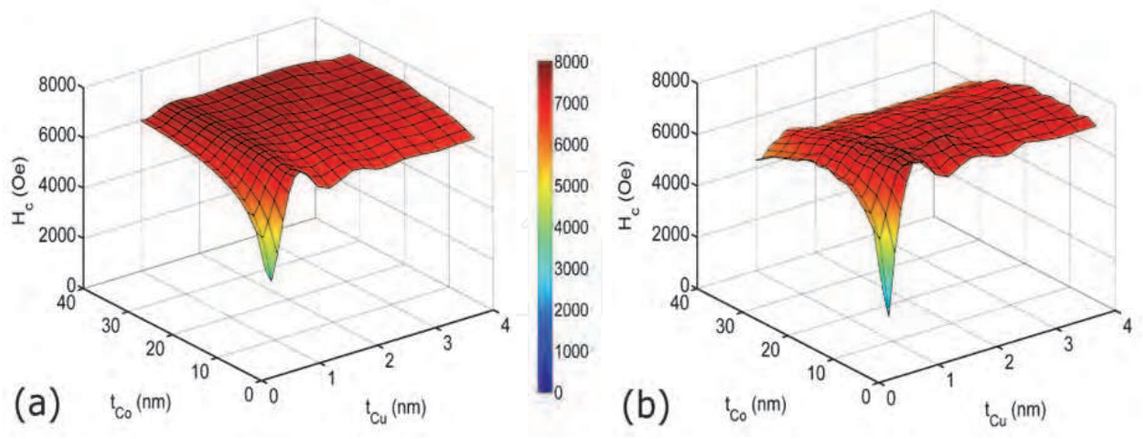

Fig. 2. Coercive field of trilayer systems of diameter 100 nm, and easy-axis oriented along the *x* direction, calculated against the thickness of the separated layers: a) values calculated by QAD, b) values simulated by OOMMF.

This argument suggests that for all the systems for which demagnetization dominates the exchange energy the QAD can be considered trustworthy independently of the easy-axis orientations of the magnets involved.

Figure 3 shows the percent error between the QAD values and the simulated data calculated in system of diameter 100 nm. At t_{Co} = 15 nm there is a cusp that marks the end of the QAD validity domain out of which the error rate increases proportionally to the aspect ratio. In systems characterized by Co layers thick a few nanometers the oscillatory nature of the exchange coupling energy affects the QAD model which still provides results with an error smaller than 5%. The rotation regime is clearly linked to the aspect ratio of the Co layer - it was observed that in systems of diameter less than 100 nm the coherency range is narrower and includes systems with Co layers thick a few nanometers; contrariwise in systems with a diameter larger than 100 nm the coherency range widens. As a conclusion, where this condition is validated, the QAD is a helpful tool to aid the choice of the proper system to be fabricated for a custom application.

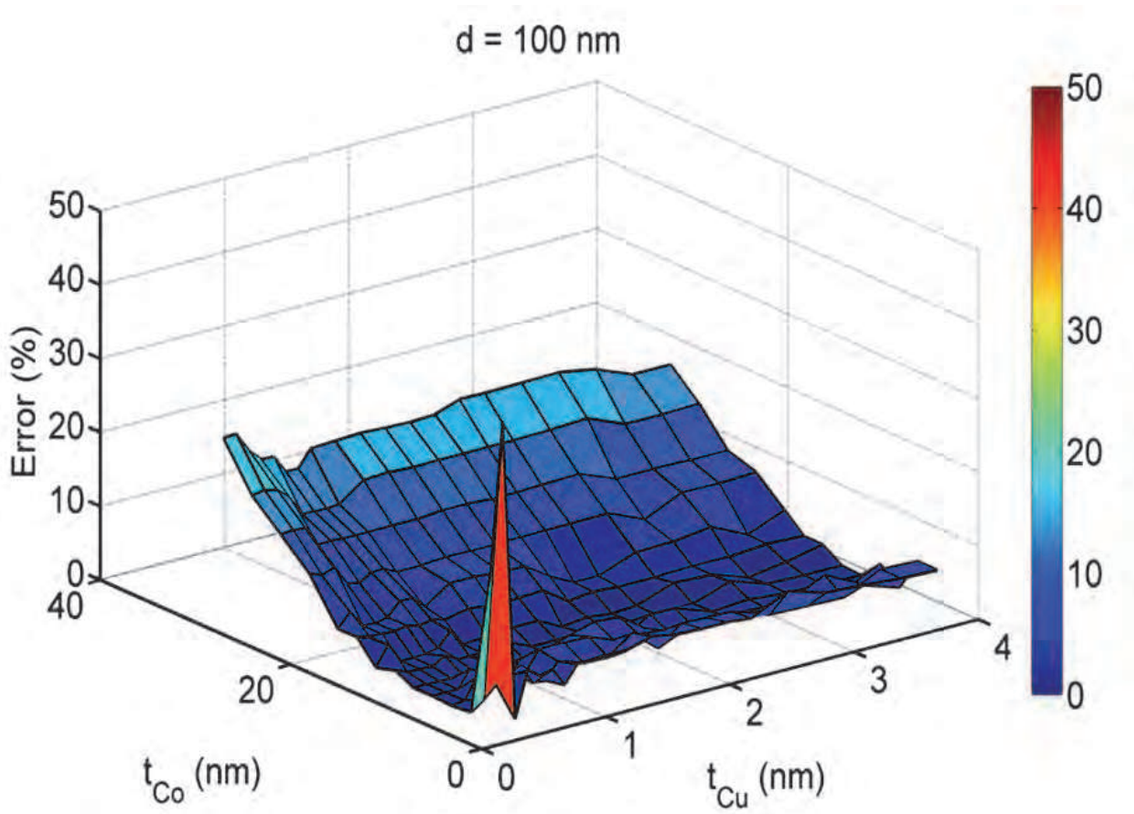

Fig. 3. Percentage error between the values calculated by QAD and simulated data for systems of diameter 100 nm and easy-axis oriented along the *x* direction.

3.2 The ZFC systems

In the present section the Co/Cu/Co trilayer systems which satisfy the ZFC are presented. In particular, the state of magnetization at zero field of cylindrical trilayer systems of diameters 50, 100 and 200 nm and easy-axis oriented along the *z* direction are reported, as a function of the layers thickness, in Figure 4.

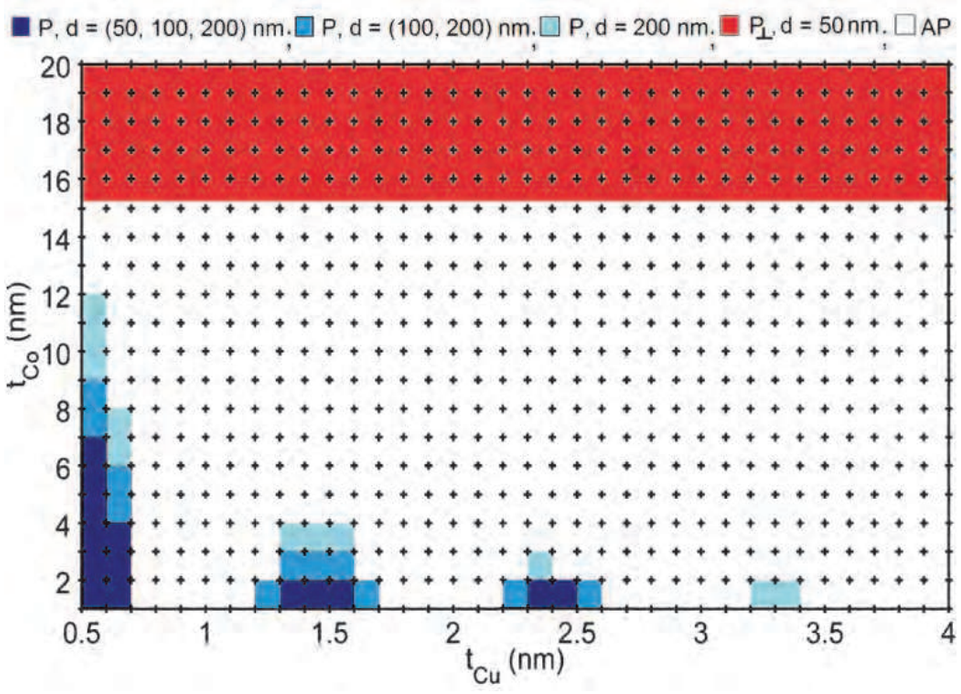

Fig. 4. State of magnetization at zero applied field of cylindrical Co/Cu/Co trilayer systems of diameters 50, 100 and 200 nm characterized by an easy-axis oriented along the *z* direction. The legend refers to different colored squares identifying the magnetization state of the cylindrical trilayer systems whose diameter is reported between brackets. The cross markers placed at the left bottom corners of the colored squares univocally intercept the thickness values of the Co and Cu layers of each system considered.

From this figure it is apparent that the trilayer systems which satisfy the ZFC are defined by selected combinations of d, t_{Cu} and t_{Co}; this fact results from the competition among the different elementary interactions taking place between two separate magnets which depend, in different fashions, on their size and shape.

The reason why only the systems characterized by the easy-axis oriented along the z-direction were considered here concerns the fact, widely acknowledged, that in such a system when the field is applied parallel to the easy-axis of magnetization the magnetization reversal is very abrupt, while when the field is applied parallel to the hard-axis, the magnetization generally rotates, gradually and in a reversible fashion, away from the easy direction (Du Trémolet de Lacheisserie et al., 2002). In this latter case, the magnetization processes involve the continuous rotation of magnetization from positive to negative saturation which is very useful for sensing purposes. Considering the current setup, to obtain systems with a analogue magnetic response is necessary to impose that the easy-axis be lined up along the *z* direction. The latter assertion is confirmed by micromagnetic simulation; the systems characterized by an easy-axis parallel to the applied-field's sweeping direction (*x* direction in our case), in most cases, can flip back and forth practically instantly from the AP to the P state of magnetization, and generally exhibit a square shaped hysteresis loop. For this reason, from here onwards, it is showed a value data-base of simulated quantities characterizing the response magnetization curve of a large number of system configurations (with easy-axis along *z* direction) to aid a prompt design of custom sensing devices.

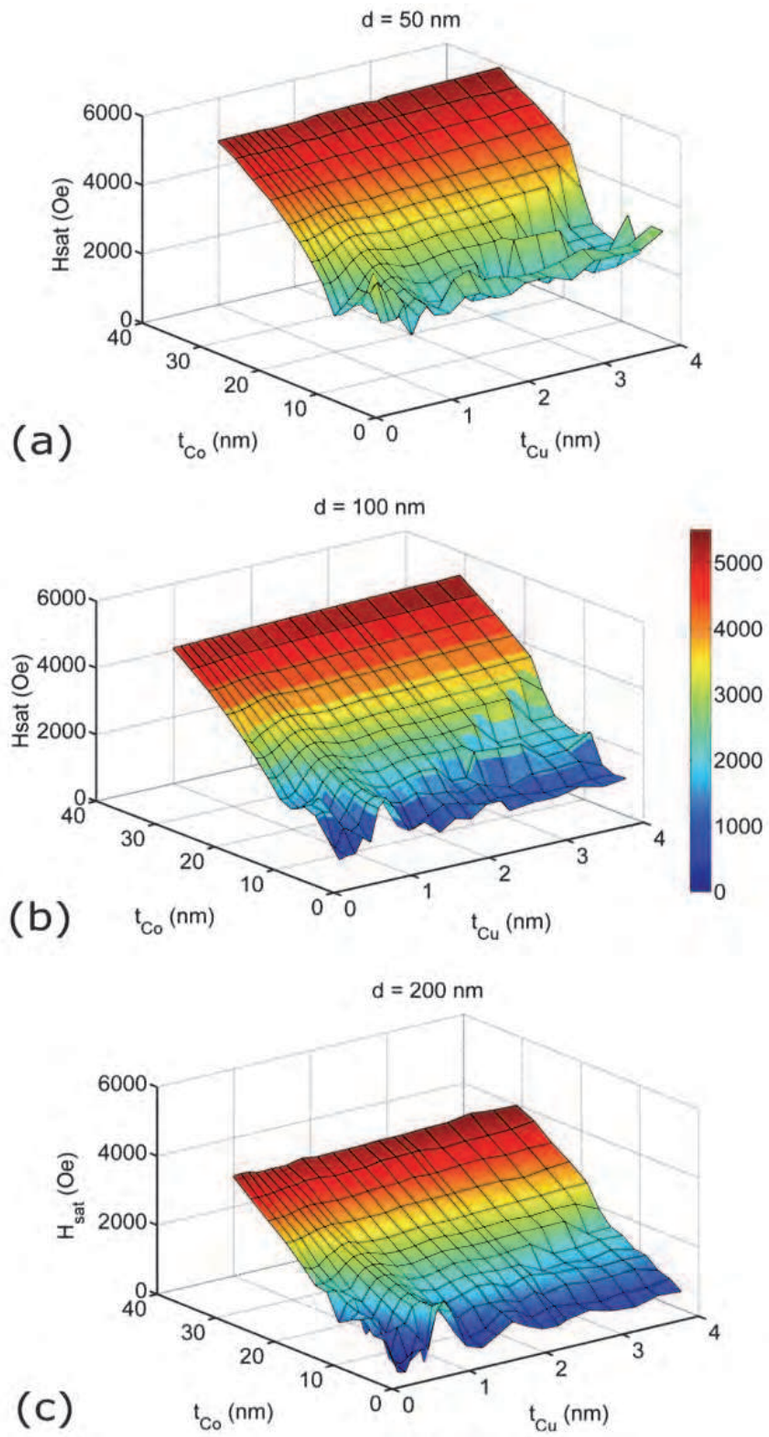

Fig. 5. Saturation field of cylindrical Co/Cu/Co trilayer systems of diameters 50, 100 and 200 nm characterized by an easy-axis oriented along the z direction. The mesh's intersection points of the 3D surface depicted correspond to the geometrical parameters of the simulated systems.

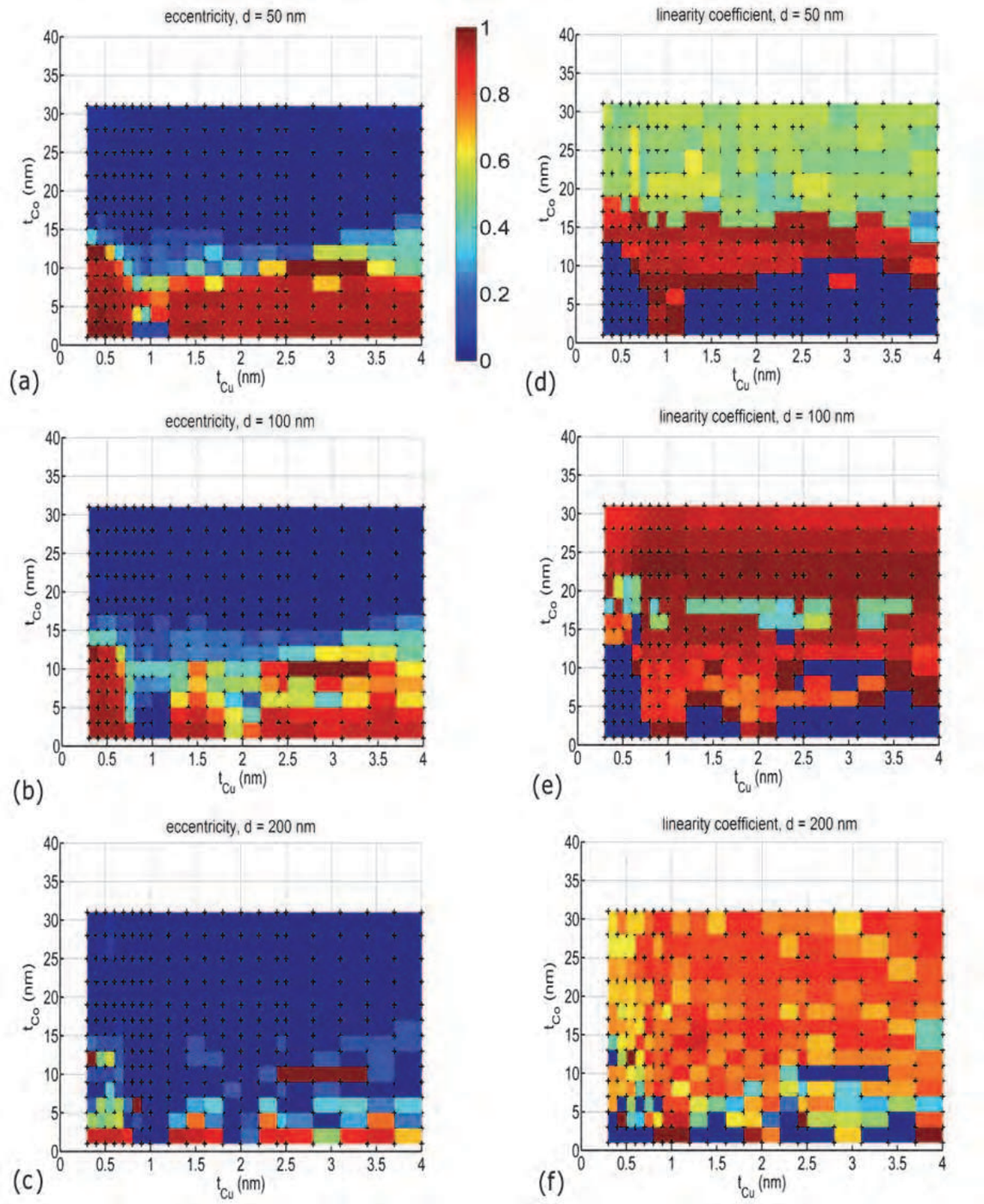

Fig. 6. Eccentricity and linearity coefficient of the magnetization curves of cylindrical Co/Cu/Co trilayer systems of diameters 50, 100 and 200 nm characterized by an easy-axis oriented along the z direction. Colors represent the value of eccentricity and linearity coefficient while the cross markers placed at the left bottom corners of the tone squares univocally intercept the thickness value of the system's Co and Cu layers.

3.3 Systems with easy-axis in the z direction

Respectively the figures 5 and 6 show, as a function of d, t_{Cu} and t_{Co}, the saturation field (H_{sat}), the eccentricity and the linearity coefficient of the magnetization curves of systems with diameters 50 nm, 100 nm and 200 nm and characterized by an easy-axis oriented along the z direction. Particularly, the eccentricity is defined here as the ratio between the intensity of the coercive and saturation fields, and the linearity coefficient is the Pearson product-moment correlation coefficient calculated from the simulated values of magnetization and the respective applied field ones within the dynamic range defined from - H_{sat} and H_{sat} (Rodgers & Nicewander, 1988). Figures 5 and 6 represent a database of parameters to choose from when a magnetic sensor of this type has to be designed for custom applications. It is apparent that, according to the envisaged application, the best design choice is a trade off among the magneto-resistive ratio, the H_{sat} (linked to the sensor dynamic range), the eccentricity and the linearity of the magnetization curve which have to be respectively minimized and maximized to avoid massive electronic post-corrections. In Figure 7 the magneto-resistive ratio of Co/Cu/Co trilayer systems, calculated from the Fert and Valet model is reported for the convenience of the sensor designer (Valet & Fert, 1993; Fert et al., 1994).

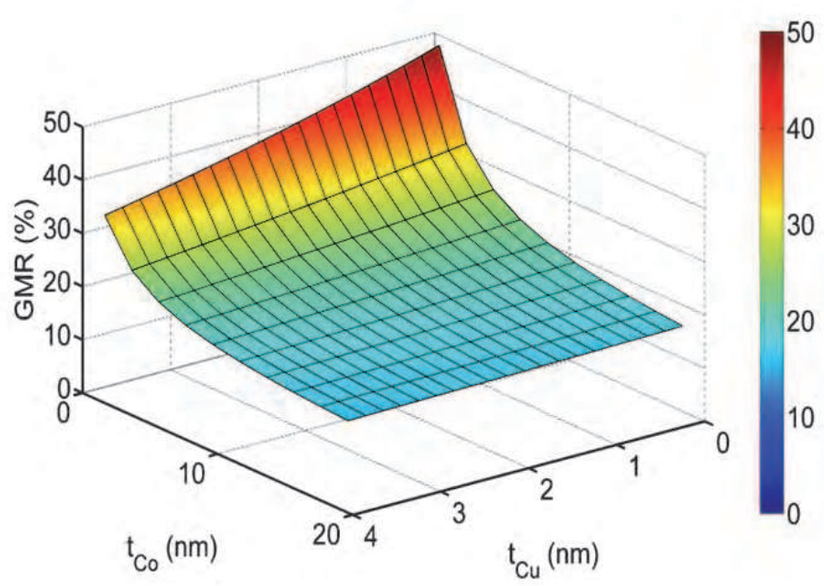

Fig. 7. Magneto-resistive ratio as a function of the Co and Cu layer thicknesses. The mesh's intersection points of the 3D surface depicted correspond to the geometrical parameters of the systems considered.

3.4 From the trilayer to the multilayers

The present chapter specifically refers to magnetic field transducers constituted by arrays of Co/Cu multilayer nanowires connected in parallel in a current perpendicular to plane (CPP) architecture. If the magneto-resistance ratio does not depend on the number of layers employed in the system, the system's critical-fields and the shape of its magnetoresistance curve depend both on the number of Co/Cu bilayers piled up to form each single nanowires

and on the presence of identical systems located in the surroundings (as for arrays of nanowires). In particular, to gauge the influence of multiple bilayers (connected either serially or in parallel) on the dynamic range of the multilayer systems is of paramount importance for the practical use of the technology addressed. Therefore, for this section, micromagnetic simulation was used to corroborate the QAD predicted properties of a large plurality of elementary trilayers (section 3.3) and to simulate the magnetic behaviour of selected bilayers interacting when forming a nanowire (up to 50 Co/Cu bilayers - hereinafter simulated multilayer system, SMS), and arranged in parallel, on the same plane, to mimic a systems' arrays (5 x 3 array). The Figure 8 represents how the layers number affects the dynamic range of a single nanowire - the dashed line represents the logarithmic best fit interpolating the simulated data (rhombus). As apparent from the plot the nanowire's saturation field increases logarithmically as a function of the elementary bilayers. As apparent from this graph, if low dynamic ranges are needed, shortest possible nanowires have to be fabricated.

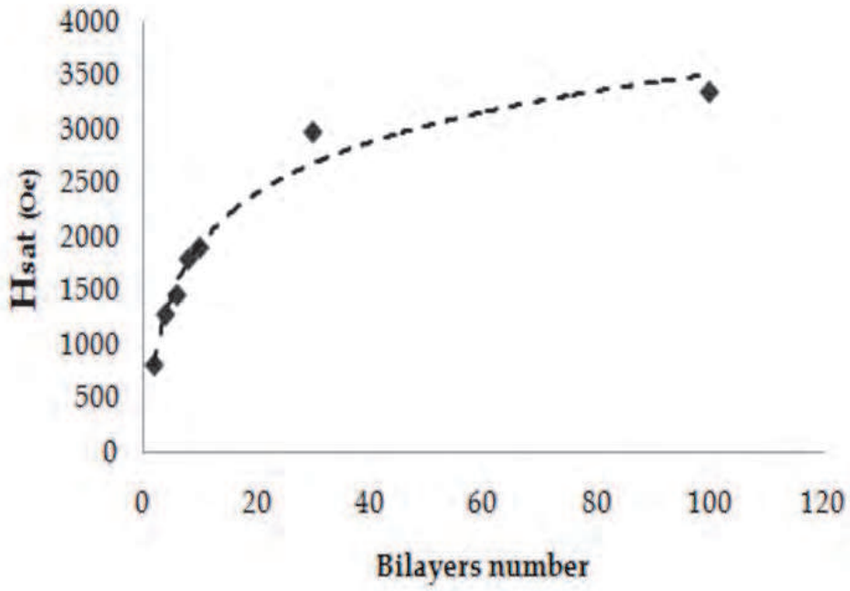

Fig. 8. Saturation magnetic field as a function of the bilayer number employed in the multilayer. The dashed line represents the logarithmic fit which best interpolates the simulated data (rhombus).

To take into account the mutual reciprocal effect of identical nanowires on the overall saturation, the magnetostatic interaction in the dipole approximation (Sun et al., 2005) was made explicit for the systems addressed. In this approximation a single nanowire is represented by a magnetic dipole characterized by a magnetization value obtained considering the contribution of each Co layer of the system; as a result, the potential energy of the interaction between two nanowires could be written as follow:

$$\mathbf{H} = -\frac{\mu_0}{4\pi r_{jk}^3}\left(3\left(\mathbf{m_j}\cdot\mathbf{e_{jk}}\right)\left(\mathbf{m_k}\cdot\mathbf{e_{jk}}\right)-\mathbf{m_j}\cdot\mathbf{m_k}\right), \tag{12}$$

where $\mathbf{m_k}$ and $\mathbf{m_j}$ are the magnetizations vector of two interacting nanowires, $\mathbf{r}_{jk}$ is their distance and $\mathbf{e_{jk}}$ is a unit vector parallel to the line joining their centers. Specifically, in this section, an array of nanowires arranged in a honeycomb configuration was considered to represent the most common array geometry encountered when using anodic porous alumina (APA, 10^{10} nanopores/cm^2) as a nanoporous template to have it fabricated. The Figure 9 shows a simplified array (hereinafter simulated array system, SAS) consisting of thirteen multilayer system of geometric and crystalline properties (d = 50 nm, t_{Co} = 2.5 nm, t_{Cu} = 2.5 nm and easy axis parallel to wire axis) used in the previous simulation.

To mimic the magnetostatic interaction of nanowires in parallel, simulations were carried out for the same SAS geometry but considering multilayers having respectively two, four, six and eight bilayers (the elementary GMR unit – one Co/Cu bilayer) each.

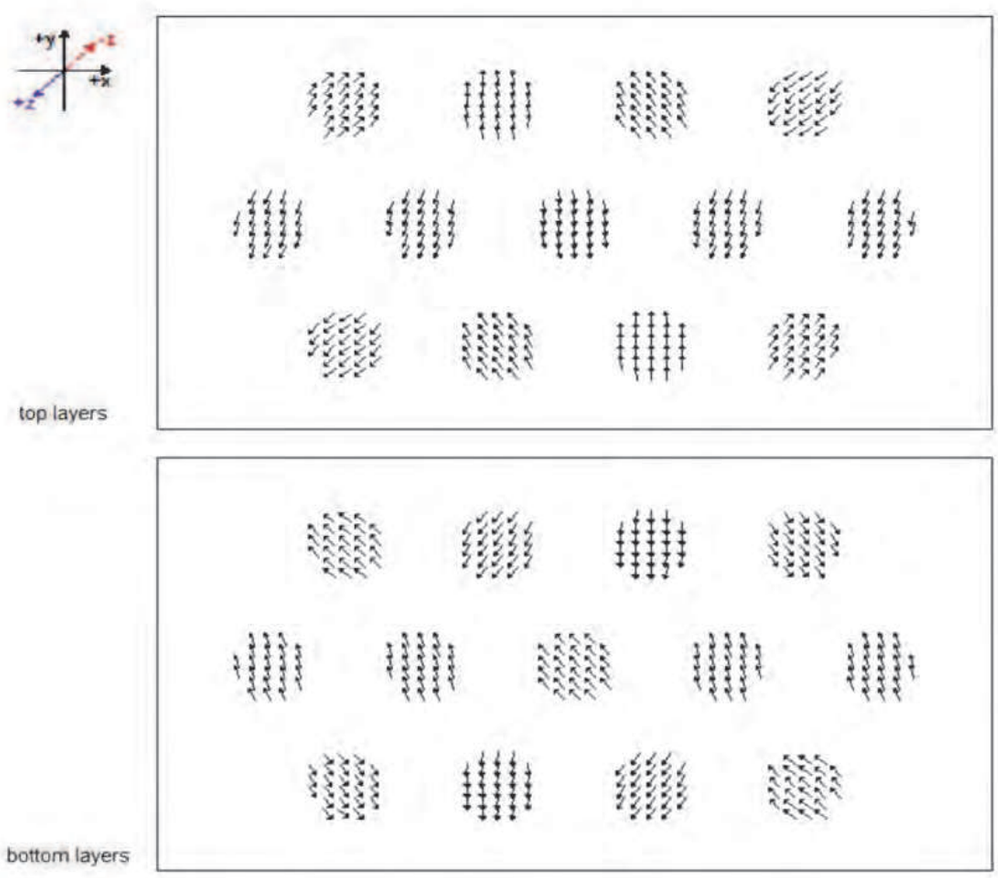

Fig. 9. An example of simulated micromagnetic configurations of the top and bottom layers of 13 trilayer systems in a honeycomb arrangement.

The Figure 10 reports the comparison of the saturation magnetic field between the SAS and the corresponding SMS as a function of the number of layers employed. As apparent in the figure the interaction between multilayers in parallel contributes to lower the saturation magnetic field. For the systems considered a maximum deviation of 10% is acknowledged.

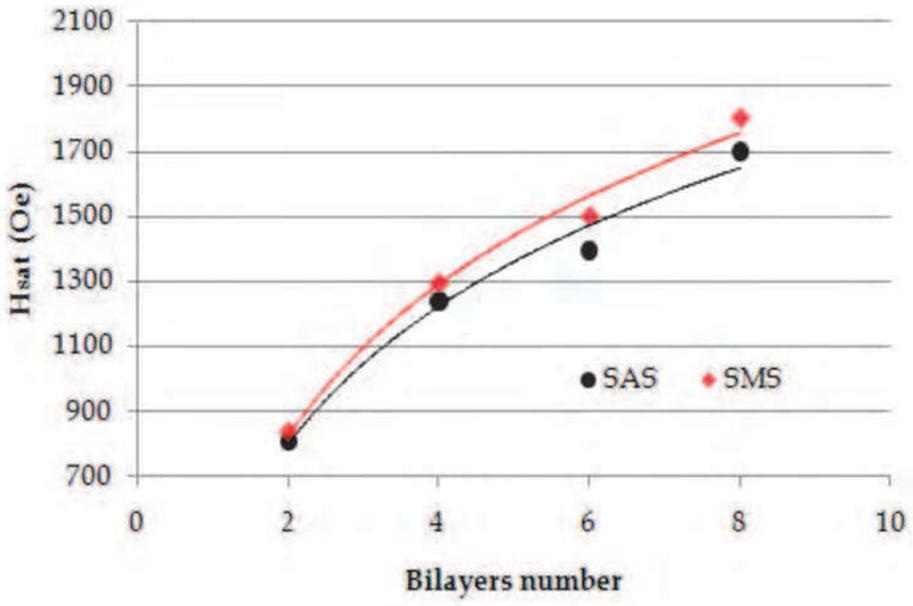

Fig. 10. Saturation magnetic field of SAS (rhombus) and SMS (circle) as a function of the number of bilayers employed each multilayer.

4. Template electrodeposition of Co/Cu-multilayer-nanowires arrays

To have Co/Cu-multilayer-nanowires arrays fabricated many approaches have being followed, among them, the chemical vapour deposition (CVD) is typically used to grow nanowires on nanocatalysts, top-down lithography and ion milling are exploited to prefabricate nanoporous membranes and lift-off masks to be filled, at a second stage, with a desired material to form nanowires and nanobelts respectively. In this context, electrodeposition has been widely utilized to fill nanoporous templates. In particular, this technique, elsewhere referred (Pullini & Busquets-Mataix, 2011) as template electrodeposition (TED) when used to fabricate single-element nanowires, or template pulsed electrodeposition (TPED) when used to fabricate multilayer nanowires, has met outstanding consideration; in fact, it is a simple method to manufacture nanomaterials on large areas both for fundamental studies and for the production of nanodevices in high volumes. Among the plethora of applications investigated, the aforementioned technique is acknowledged as being promising to mass produce magnetic-field sensors (Manalis et al., 1995; Chou et al., 1994; Simonds, 1995). The present section refers specifically to the use of the TPED for the fabrication of Co/Cu-multilayer-nanowire arrays exhibiting Giant Magnetoresistance (GMR) and in particular to provide a user with growth process parameters sized up to obtain system of desired characteristics. The conventional GMR systems are developed by vacuum techniques which require sophisticated and expensive equipments to be adopted; on the contrary, the TPED simply requires a galvanic cell controlled by a low-cost potentiostat. The simplicity of this technology is considered a great advantage for industrialization; therefore, for this reason, the main objective of the present section is to detail the TPED process to pave the way for the mass production of multilayer-nanowire-array (for CPP architecture).

4.1 Process mastering for tailoring growth

By TPED each material building multilayer nanowires arrays can be deposited by applying the proper voltage to the cell (voltage cycling). The single bath technique consists in using a single electrolytic bath made with salts of both the metal ions to be deposited, where the ion-concentration ratio is highly unbalanced towards the less noble metal (Piraux et al., 1994; Blondel et al., 1994; Evans et al., 2000; Fert & Piraux, 1999; Ohgai et al., 2003; Liu et al., 1995). As Cu deposits at a lower negative potential than Co, the former is the nobler element, therefore, its concentration in the deposition solution has to be smaller. As a consequence of that, 100% purity copper can be deposited but traces of Cu are also deposited within the Co deposition step. According to the Co purity desired one can tailor the ratio of the species present in the galvanic bath. In this specific context, the Cu impurity contents in the Co layers badly affect the magnetic properties of Co, therefore, from the application standpoint the Cu precursor in the bath has to be lowered to the minimum. On the contrary, the smaller the Cu concentration is, the slower the growth of the Cu layers. As a matter of fact, the optimal Cu concentration was chosen from a trade off between a cost-effective fabrication throughput and the GMR performance of the multilayer stack. In this work, the electrolyte used was a sulphate bath prepared by dissolving 520 g/l (1.85 mol/l) of $CoSO_4.7H_2O$, 5.2 g/l (0.021 mol/l) of $CuSO_4.5H_2O$, and 52 g/l (0.84 mol/l) of H_3BO_3. The latter compound was added to buffer the pH of the electrolytic solution to an approximate constant value of 4.5 throughout the deposition duration. These values result in a ion concentration ratio $[Co^{2+}]:[Cu^{2+}]$ of about 90 to 1. Analytical grade chemicals and purified water with a resistivity higher than 16.8 MΩ cm were used throughout.

Two different types of templates are commonly used in the art, namely the ion-track etched (TE) polymers and the anodic porous alumina membranes. Although both membrane types can provide nanochannels tailored to a given diameter, their nature and morphology present some important differences influencing the filling process and, therefore, they must be considered with particular attention (Ohgai et al., 2003; Schönenberger et al., 1997; Ferain & Legras, 2001; Pullini et al., 2007a).

Even though it is commonly acknowledged from an industrialization standpoint that TPED is a cost-effective technique and easily scalable, mainly due to a wide plurality of factors affecting the nanowire growth, there are still contradicting process details in the published literature which make the technology not ready yet to be scaled up. In fact, there are great deal of process variables which influence the electrodeposition to a higher or lesser degree: concentration of species, pH, presence of complexants and/or, brighteners, temperature, voltage and current cycling, and the membrane used (material, pore diameter and length). Today a systemic analysis of TPED taking into account these variables is still missing.

Multilayer nanowires were then fabricated alternating square-pulse potentials by the computer controlled potentiostat AMEL 500 by using a three-electrode cell, properly designed to host flexible polycarbonate TE-templates, was made of PTFE. A Pt grid was employed as a counter electrode and a saturated calomel electrode (SCE) as the reference one. In Figure 11 is shown the architecture of the experiment (a, b and c) and the typical potential driving cycle used in the process (d) with the corresponding current-density cycle (e). The open end of nanopores was arranged to face upwards, i.e. anode over cathode configuration (Konishi et al., 2003) and the deposition area was of 2 cm^2. Prior to deposition, when the nanoporous membranes were arranged properly, the cell was placed in an ultrasonic agitation bath always for 5 minutes to allow the complete wetting of the

membranes' nanopores. As reported elsewhere (Schönenberger et al., 1997), here we corroborate that this sonication time is sufficient to have the complete filling of the nanopores allowing a homogeneous growth of nanowires over the whole exposed area. The deposition was carried out at room temperature without stirring. As a result, the complete filling of the nanopores, resulting in the maximum fabrication rate of nanowires, could be achieved with success by TPED.

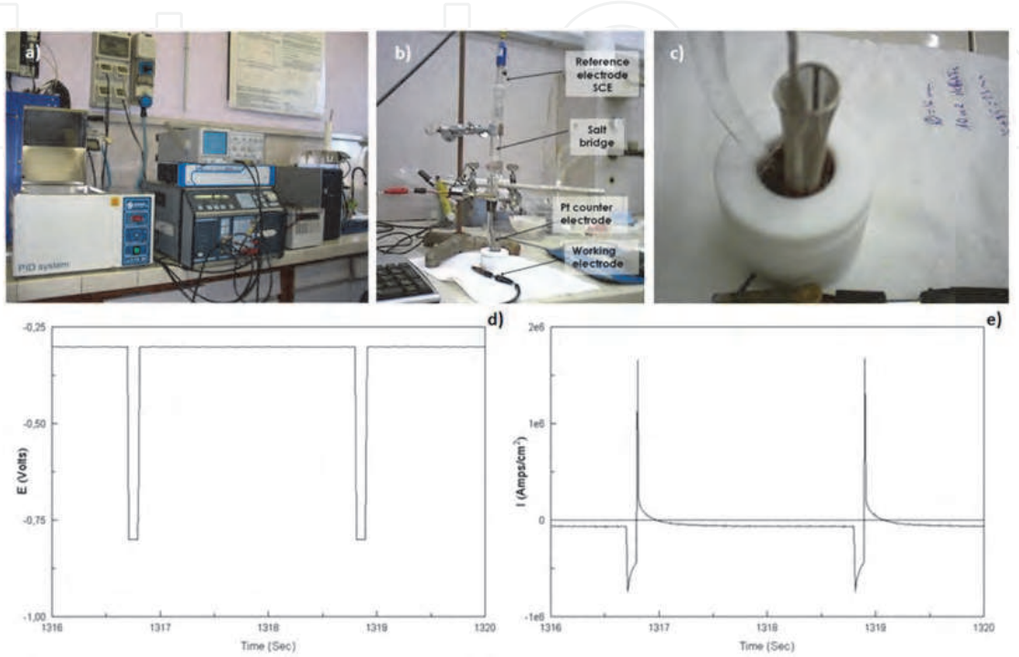

Fig. 11. (a) AMEL 500 potentiostat; (b) 3-electrodes electrodeposition cell; (c) PTFE cell detail; (d) a typical potential driving cycle (-0.3V for Cu deposition and -0.8V for Co deposition); (e) the corresponding current-density cycle.

For this section arrays of Co/Cu multilayer nanowires of 30, 50, and 100 nm diameters have been fabricated in order to provide a sensor developer with precise values for the most important growth process parameters to be used to tailor the geometry characteristics of the multilayer systems desired, particularly the layers' thickness. To this end, knowing the current efficiency of Co and Cu when deposited in alternate fashion by TPED is of fundamental importance to know the relationship between the deposition timing and the mass deposited to form each layer. In fact, by the Faraday's law the electrical charge employed within each deposition cycle is directly linked to mass deposited each layers if a 100% current efficiency is assumed. D. Pullini and D. Busquets-Mataix (Pullini & Busquets-Mataix, 2011) discusses the influence of the space confinement on the TPED and report the calculated values of current efficiencies used here to calculate the layer thicknesses to build nanowires of tailored characteristics. In this work, the current efficiencies of Co and Cu in nanotemplates were determined by the following method. The single layer volumes, which, at constant charge load, have to be theoretically invariant along the nanowire length, were determined by microscopy direct measurements of the layer diameters, tilt angle, and thicknesses. For each sample, a large number of layers belonging to central portions of nanowires were considered and the mean value of the volumes deposited each metal layer

calculated. The average layer masses of Cu and Co were obtained and compared with those calculated theoretically by the Faraday's law after integrating the current recorded over the time interval of the corresponding deposition steps. The Co anodic peaks taking place at the beginning of the following Cu deposition cycles were not taken into account. In doing so, the theoretical to real deposition value could be directly compared. Finally, the current efficiencies of Cu and Co were calculated as the ratio between the measured values of layer mass and the theoretical ones. As the nanowires fabricated for this work present the narrowest distribution of layer diameters and thicknesses in correspondence of their central parts, therefore for the present analysis, only those ones were considered (Pullini et al., 2007b). Following the chemical dissolution of the polycarbonate membranes, the morphology analysis of the nanowires was performed by TEM and complemented in some cases with scanning electron microscopy. As explained elsewhere different methods to enhance the contrast between layers for a more accurate measurement were used (Pullini et al., 2007a). The time evolution of the current efficiencies of Co and Cu in the TPED is shown by the figure 4 of Pullini and Busquets-Mataix (Pullini & Busquets-Mataix, 2011) manuscript. Both for Co and Cu cases, one can observe a slight reduction of the current efficiency when longer deposition duration is experienced. More in depth, during short deposition cycles, cations are abundant in solution, the TPED is charge controlled and the growth rate is only limited by the rapidity which ions can be chemically reduced at the interface. For the shortest deposition cycles in fact the process only depends on the applied potential irrespectively of the diameter of pores to be filled. A possible explanation of this fact is the change of the deposition conditions due to the variation of the membrane polarization provoked by the potential alternation. In fact, the membrane polarization change affects the double-layer characteristics, and the migration and diffusion of ions, somehow resulting similar to those of a space-unconfined deposition. As a main results, it was shown that the current efficiency of Cu measured for all the potential range addressed here in the TPED mode is very close to 100%; instead, it is apparent for Co that a consistent reduction has been observed – the Co TPED efficiency ranges between 60% to nearly 70%. In a first instance, the significant reduction of Co current efficiency could be accounted as a re-dissolution of Co during the Cu deposition cycle (Valizadeh et al., 2002). This hypothesis is corroborated by the presence of a high anodic peak observed at the beginning of each Cu deposition cycle - the peak shows itself in the first instants after the potential switches. Co dissolution can drastically change the actual layer thicknesses with respect to the nominal values deduced from Faraday's law (V. Weihnacht et al. 2003; Bakonyi & Péter, 2010), and therefore, the direct measurement method presented in the manuscript is fairly suited to ascertain the real deposition efficiencies in multilayered nanowires. This peak can be reduced by the adequate selection of the Cu deposition potential as showed by Liu et al. (Liu et al., 2004) and Péter et al. (Péter et al., 2004) to higher absolute values (i.e. -0.6V). From the fact that the pore diameter does not play a significant role on the Co and Cu current efficiencies in the TPED mode and form the measured values of the current efficiencies reported in D. Pullini and D. Busquets-Mataix (D. Pullini & D. Busquets-Mataix, 2011) a growth parameter data base, to promptly allow a user to fabricated a Co/Cu multilayer nanowires array of tailored properties, the electric charge to be employed for deposit the material thickness desired to build the single layers of the array is given in this section as a function of the deposition potential.

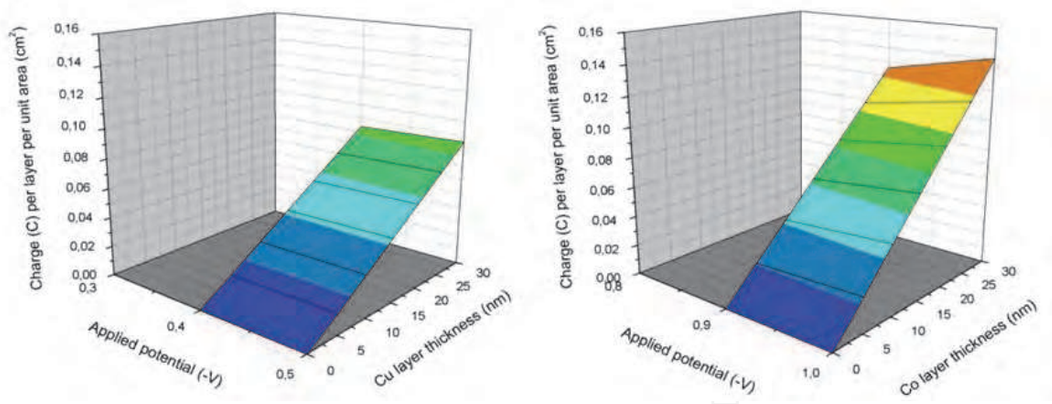

Fig. 12. Charge per cycle per unit area as a function of the electrode potentials to deposit Cu (left) and Co (right) in TPED.

In fact, using Figure 12 the electrode potential for Cu (left graph) and Co (right graph) in TPED is directly linked to the thickness desired of the single layer of either Co or Cu, the charge per cycle and per unit area is reported, and makes straightforward the use of TPED for the purpose. It is important to notice that the area to be considered for calculations is the effective area, i.e. not the area of the membrane wetted by the electrolyte but the product of the area of a single hole times the density of holes in the membrane. In these, current efficiency for Cu deposition was close to 100% whereas for Co deposition varied from 60% to 70%, being these differences mainly related to applied potential. A detailed discussion of the Co and Cu current efficiencies either when the elements are deposited in constant or in alternate mode is reported as a function of the respective electrode potentials and the deposition duration. [ref: Pullini, D.; Busquets, D.; (2011). Electrodeposition Efficiency of Co and Cu in the Fabrication of Multilayer Nanowires by Polymeric Track-Etched Templates. ACS Appl. Mater. Interfaces, 3 (3), pp 759–764- DOI: 10.1021/am1011222]

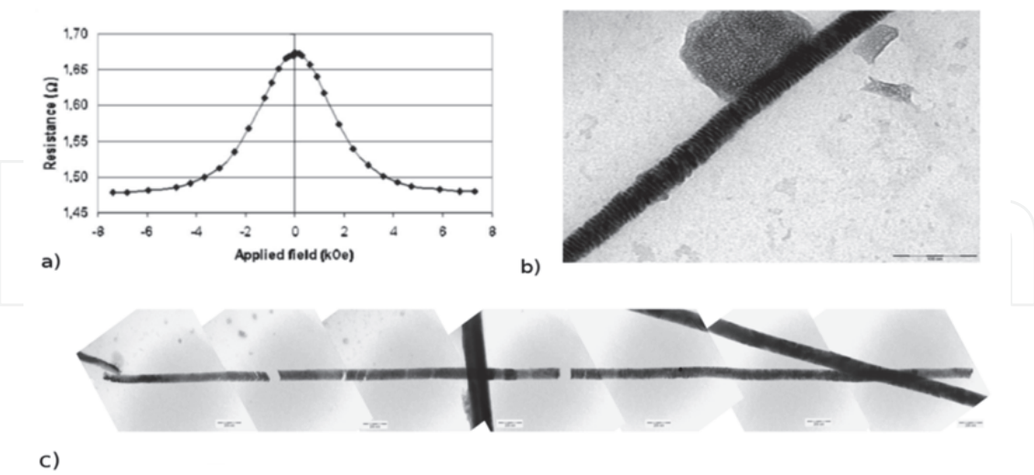

Fig. 13. (a) Magnetoresistive response of arrays of Co/Cu nanowire of 50 nm diameter; (b) TEM imagine of 60 nm diameter Co/Cu multilayer nanowire; (c) TEM image of an 100 nm diameter Co/Cu multilayer nanowire – in-full collage.

GMR measurements were carried out by a four-contact method on each sample fabricated for the study. A thin layer of gold was sputtered on the top side of the template membrane

to ensure the electrical continuity. Magnetic field was applied orthogonally to the wire axes according to a conventional CPP configuration, whereas current flows along the wire axes. Saturation was always reached and GMR was calculated as $\Delta R/R_{max}$ (Fert & Piraux, 1999). A typical magnetoresistance to field curve is presented in Figure 13 where are also two TEM images of a Co/Cu multilayer nanowire of GMR properties.

5. Conclusions

In this chapter a quasi-analytical method to predict the magnetic properties of trilayer systems to aid the design of magnetic field sensors has been defined. In particular, the authors addressed here Co/Cu/Co trilayer systems of cylindrical shape to have an insight into the magnetic behaviour of more complex Co/Cu nanowire systems frequently reported in the literature for said purposes. The interest in Co/Cu multilayer nanowires is motivated by the fact that their properties are relatively easy to be tailored by controlling the process parameters if electrodeposition into nanoporous templates is used to have them grown. The QAD consists of defining and solving the total energy problem of these systems as a function of the trilayers diameter, the layers thickness and the crystal orientation of the materials used. The total energy of the system is built from the analytical expressions of all the involved energy terms except the demagnetization one whose expression is a function of the values, calculated numerically, which the demagnetization energy assumes when the system is in four fundamental states of magnetization. A large number of trilayer systems differing in d (50, 100 and 200 nm), **a** (oriented along the x and z axis), t_{Co} (ranging from 0 and 40 nm), and t_{Cu} (ranging from 0 to 4 nm) have been analyzed by this method. For all these systems, the micromagnetic simulation has been used to understand when the assumption of coherent rotation of the single magnetic moments belonging to the separate layers is valid. For the reasons explained, we can assume that in system with 100 nm of diameter when the Co layers are thinner than 15 nm the single dipoles rotate coherently and the QAD predictions fully match the simulation values. Instead, for larger t_{Co} the QAD is still trustworthy at predicting qualitatively the magnetization reversal process although discrepancies in the absolute values of H_c are acknowledged. At last, a data-base of values of simulated quantities which characterize the response magnetization curve is given for a large number of system configurations to aid a prompt design of custom sensing devices. Nevertheless, from the precise estimation for current efficiency of Co and Cu in TPED mode the growth-process parameters to tailor the morphology of custom systems have been detailed to provide a sensor developer with fundamental data to have GMR–nanowires array system fabricated.

6. References

Simonds, J. L. (1995). Magnetoelectronics: Today and Tomorrow. *Physics Today*, Vol.48, No.4, (April 1995), pp. 26-30, ISSN 0031-9228

Grünberg, P.; Schreiber, R.; Pang, Y.; Brodsky, M. B. & Sowers, H. (1986). Layered Magnetic Structures: Evidence for Antiferromagnetic Coupling of Fe Layers across Cr Interlayers. *Phys. Rev. Lett.*, Vol.57, No.19, (September 2009) pp. 2442-2445, ISSN 0031-9007

Saurenbach, F.; Walz, U.; Hinchey, L.; Grünberg, P. & Zinn, W. (1988). Static and dynamic magnetic properties of Fe-Cr-layered structures with antiferromagnetic interlayer exchange. *J. Appl. Phys.*, Vol.63, No.8, (May 1988), pp. 3473-3476, ISSN 0021-8979

Baibich, M. N.; Broto, J. M.; Fert, A.; Nguyen Van Dau, F. & Petroff, F. (1988). Giant Magnetoresistance of (001)Fe/(001)Cr Magnetic Superlattices, *Phys. Rev. Lett.*, Vol.61, No.21, (August 1988), pp. 2472-2475, ISSN 0031-9007

Manalis, S.; Babcock, K.; Massie, J.; Elings, V. & Dugas, M. (1995). Submicron studies of recording media using thin-film magnetic scanning probes. *Appl. Phys. Lett.*, Vol.66, No.19, (May 1995), pp. 2585-2587, ISSN 0003-6951

Chou, S. Y.; Wei, M. S.; Krauss, P. R. & Fisher, P. B. (1994). Single-domain magnetic pillar array of 35 nm diameter and 65 Gbits/in.^{2} density for ultrahigh density quantum magnetic storage. *J. Appl. Phys.*, Vol.76, No.10, (1994), pp. 6673-6675, ISSN 0021-8979

Pullini, D.; Innocenti, G.; Busquets, D. & Ruotolo, A. (2007a). Investigation of multilayer local tilt within long portion of single Co/Cu nanowires. *Appl. Phys. Lett.*, Vol.90, No.13 (October 2006), pp. 133106-133106-3 , ISSN 0003-6951

Fert, A. & Piraux, L. (1999). Magnetic nanowire. *J. Magn. Magn. Mat.*, Vol.200, No.1-3, (March 1999), pp. 338-358, ISSN 0304-8853

Piraux, L.; George, J.M.; Depres, J.F.; Leroy, C.; Ferain, E.; Legras, R.; Ounadjela, K. & Fert, A. (1994). Giant magnetoresistance in magnetic multilayered nanowires. *Appl. Phys. Lett.*, Vol.65, No.19, (November 1994), pp. 2484-2486, ISSN 0003-6951

Ohgai, T.; Hoffer, X.; Gravier, L.; Wegrowe, J. E. & Ansermet, J.-Ph. (2003). Bridging the gap between template synthesis and microelectronics: spin-valves and multilayers in self-organized anodized aluminum nanopores. *Nanotechnology,* Vol.14, Issue 9, (September 2003), pp. 978-982, ISSN 0957-4484

Sun, L.; Hao, Y.; Chien, C.L. & Searson, P.C. (2005). Tuning the properties of magnetic nanowires. *IBM Journal of Research and Development*, Vol.49, No.1, (January 2005), pp. 79-102, ISSN 0018-8646

Bruno, P. & Chappert, C. Oscillatory coupling between ferromagnetic layers separated by a nonmagnetic metal spacer. *Phys. Rev. Lett.*, Vol.67, No.12 (June 1991), pp. 1602-1605, ISSN 0031-9007

Du Trémolet de Lacheisserie, É.; Gignoux, D. & Schlenker, M. (2002). *Magnetism II: Materials and Applications*, Kluwer Academic Publishers, ISBN 1402072236, Norwell

Rodgers, J. L. & Nicewander, W. A. (1988). Thirteen ways to look at the correlation coefficient. *The American Statistician*, Vol.42, No.1, (February 1988), pp. 59-66, ISSN 0003-1305

Valet, T. & Fert, A. (1993). Theory of the perpendicular magnetoresistance in magnetic multilayers, *Phys. Rev. B*, Vol.48, No.10, (April 1993), pp. 7099-7113, ISSN ISSN 1550-235X

Fert, A.; Valet, T. & Barnas, J. (1994). Perpendicular magnetoresistance in magnetic multilayers: Theoretical model and discussion (invited). *J. Appl. Phys.*, Vol.75, No.10, (May 1994), pp. 6693-6698, ISSN 0021-8979

Pullini, D. & Busquets-Mataix, D. (2011). Electrodeposition Efficiency of Co and Cu in the Fabrication of Multilayer Nanowires by Polymeric Track-Etched Templates. *ACS Appl. Mater. Interfaces*, Article ASAP Publication Date (Web): February 22, 2011

Blondel, A.; Meier, J. P.; Doudin, B. & Ansermet, J. Ph. (1994). Giant magnetoresistance of nanowires of multilayers. *Appl. Phys. Lett.*, Vol.65, No.23, (July 1994), pp. 3019-3021, ISSN 0003-6951

Evans, P. R.; Yi, G. & Schwarzacher, W. (2000). Current perpendicular to plane giant magnetoresistance of multilayered nanowires electrodeposited in anodic aluminum oxide membranes. *Appl. Phys. Lett.*, Vol.76, No.4, (June 1999), pp. 481-483, ISSN 0003-6951

Liu, K.; Nagodawithana, K.; Searson, P.C. & Chien, C.L. (1995). Perpendicular giant magnetoresistance of multilayered Co/Cu nanowires. *Phys. Rev. B*, Vo.51, No.11, (November 1994), pp. 7381-7385, ISSN 1550-235X

Ferain, E. & Legras, R. (2001). Pore shape control in nanoporous particle track etched membrane. *Nucl. Instrum. Methods Phys. Res. B*, Vol.174, No.1-2, (September 2000), pp. 116-122, ISSN 0168-583X

Konishi, Y.; Motoyama, M.; Matsushima, H.; Fukunaka, Y.; Ishii, R. & Ito, Y. (2003). Electrodeposition of Cu nanowire arrays with a template. *J. Electroanal. Chem.*, Vol.559, (February 2003), pp. 149-153, ISSN 1572-6657

Schönenberger, C.; van der Zande, B. M. I.; Fokkink, L. G. J.; Henny, M.; Schmid, C.; Krüger, M.; Bachtold, A.; Huber, R.; Birk, H. & Staufer, U. (1997). Template Synthesis of Nanowires in Porous Polycarbonate Membranes: Electrochemistry and Morphology. *J. Phys. Chem. B,* Vol.101, No.28, (March 1997), pp. 5497-5505, ISSN 1089-5647

Pullini, D.; Busquets, D.; Ruotolo, A.; Innocenti, G. & Amigo, V. (2007b). Insights into pulsed electrodeposition of GMR multilayered nanowires. *J. Magn. Magn. Mater.*, Vol.316, No.2, (September 2007), pp. e242–e245, ISSN 0304-8853

Valizadeh, S.; George, J. M.; Leisner, P. & Hultman, L. (2002). Electrochemical synthesis of Ag/Co multilayered nanowires in porous polycarbonate membranes. *Thin Solid Films*, Vol.402, No.1-2, (September 2001), pp. 262–271, ISSN 0040-6090

V. Weihnacht, V.; Péter, L.; Tóth, J.; Pádár, J.; Kerner, Zs.; Schneider, C.M. & Bakonyi, I. (2003). Giant Magnetoresistance in Co-Cu/Cu Multilayers Prepared by Various Electrodeposition Control Modes. *J Electrochem. Soc.*, Vol.150, No.8, (February 2003), pp. C507-C515, ISSN 1945-7111

Bakonyi, I. & Péter, L. (2010). Electrodeposited multilayer films with giant magnetoresistance (*GMR*): Progress and problems. *Progr. Mater. Sci.*, Vol.55, No.3, (July 2009), pp. 107-245, ISSN 0079-6425

Liu, Q.X.; Péter, L.; Tóth, J.; Kiss, L.F.; Cziráki, Á. & Bakonyi, I. (2004). The role of nucleation in the evolution of giant magnetoresistance with layer thicknesses in electrodeposited Co–Cu/Cu multilayers. *J. Magn. Magn. Mater.*, Vol.280, No.1, (February 2004), pp. 60-74, ISSN 0304-8853

Péter, L.; Liu, Q.X.; Kerner, Zs. & Bakonyi, I. (2004). Relevance of the potentiodynamic method in parameter selection for pulse-plating of Co–Cu/Cu multilayers. *Electrochimica Acta*, Vol.49, No.9-10, (November 2003), pp. 1513-1526, ISSN 0013-4686

Nanowires - Implementations and Applications

Edited by Dr. Abbass Hashim

ISBN 978-953-307-318-7
Hard cover, 538 pages
Publisher InTech
Published online 18, July, 2011
Published in print edition July, 2011

This potentially unique work offers various approaches on the implementation of nanowires. As it is widely known, nanotechnology presents the control of matter at the nanoscale and nanodimensions within few nanometers, whereas this exclusive phenomenon enables us to determine novel applications. This book presents an overview of recent and current nanowire application and implementation research worldwide. We examine methods of nanowire synthesis, types of materials used, and applications associated with nanowire research. Wide surveys of global activities in nanowire research are presented, as well.

How to reference

In order to correctly reference this scholarly work, feel free to copy and paste the following:

Daniele Pullini, David Busquets Mataix and Alessio Tommasi (2011). Co/Cu Nanowire Systems for GMR Sensing Applications, Nanowires - Implementations and Applications, Dr. Abbass Hashim (Ed.), ISBN: 978-953-307-318-7, InTech, Available from: http://www.intechopen.com/books/nanowires-implementations-and-applications/co-cu-nanowire-systems-for-gmr-sensing-applications

INTECH
open science | open minds

InTech Europe
University Campus STeP Ri
Slavka Krautzeka 83/A
51000 Rijeka, Croatia
Phone: +385 (51) 770 447
Fax: +385 (51) 686 166
www.intechopen.com

InTech China
Unit 405, Office Block, Hotel Equatorial Shanghai
No.65, Yan An Road (West), Shanghai, 200040, China
中国上海市延安西路65号上海国际贵都大饭店办公楼405单元
Phone: +86-21-62489820
Fax: +86-21-62489821

IntechOpen